analytical chemistry

ARTICLE

pubs.acs.org/ac

Simulation and Experimental Studies on Plasma Temperature, Flow Velocity, and Injector Diameter Effects for an Inductively Coupled Plasma

Helmut Lindner,[*,†] Ayrat Murtazin,[‡] Sebastian Groh,[§] Kay Niemax,[‡] and Annemie Bogaerts[†]

[†]Plasma, Laser Ablation and Surface Modelling Antwerp, Department of Chemistry, University of Antwerp, Universiteitsplein 1, 2610 Antwerpen, Belgium

[‡]Department Analytical Chemistry and Reference Materials, Federal Institute for Materials Research and Testing, Berlin, Germany

[§]Leibniz Institute for Analytical Sciences, Dortmund, Germany

Supporting Information

ABSTRACT: An inductively coupled plasma (ICP) is analyzed by means of experiments and numerical simulation. Important plasma properties are analyzed, namely, the effective temperature inside the central channel and the mean flow velocity inside the plasma. Furthermore, the effect of torches with different injector diameters is studied by the model. The temperature inside the central channel is determined from the end-on collected line-to-background ratio in dependence of the injector gas flow rates. Within the limits of 3% deviation, the results of the simulation and the experiments are in good agreement in the range of flow rates relevant for the analysis of relatively large droplets, i.e., ∼50 μm. The deviation increases for higher gas flow rates but stays below 6% for all flow rates studied. The velocity of the gas inside the coil region was determined by side-on analyte emission measurements with single monodisperse droplet introduction and by the analysis of the injector gas path lines in the simulation. In the downstream region significantly higher velocities were found than in the upstream region in both the simulation and the experiment. The quantitative values show good agreement in the downstream region. In the upstream region, deviations were found in the absolute values which can be attributed to the flow conditions in that region and because the methods used for velocity determination are not fully consistent. Eddy structures are found in the simulated flow lines. These affect strongly the way taken by the path lines of the injector gas and they can explain the very long analytical signals found in the experiments at low flow rates. Simulations were performed for different injector diameters in order to find conditions where good analyte transport and optimum signals can be expected. The results clearly show the existence of a transition flow rate which marks the lower limit for effective analyte transport conditions through the plasma. A rule-of-thumb equation was extracted from the results from which the transition flow rate can be estimated for different injector diameters and different injector gas compositions.

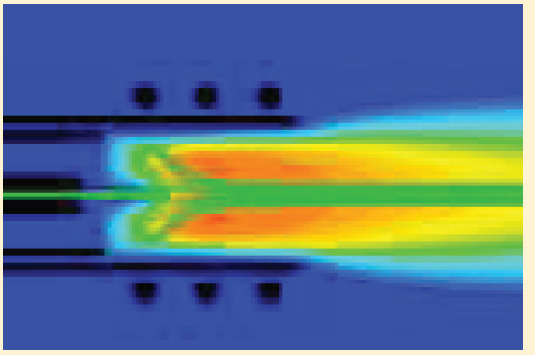

Inductively coupled plasmas (ICP) are widely used excitation and ion sources for elemental analysis in analytical chemistry. They are usually coupled to optical emission spectroscopic (OES) or mass spectroscopic (MS) detection systems; see, e.g., refs 1−3. The sample is usually delivered by liquid nebulization through the injector tube into the ICP. Different kinds of nebulizers are available, and large droplets are typically removed from the aerosol that is transferred to the ICP via spray chambers.[4] However, also direct injection high-efficiency nebulizers (DIHEN) are applied. They produce larger droplets than other nebulizers, but they require only a lower sample gas flow rate and produce the droplets just in front of the plasma, which provides a relatively high sample introduction efficiency.[5] Another method for sample delivery is laser ablation (LA), where a solid sample is irradiated by a pulsed laser and the particles formed from the ablated material are transported by a gas stream into the ICP.[6] Furthermore, single droplets have been used for sample introduction of dissolved analytes as well as suspended nanoparticles, desolvated particles, and cells.[7−10]

The single-droplet introduction is a promising technique because it allows one to use only small amounts of analyte solution or suspension. Additionally, the sample introduction efficiency is 100% (see Groh et al.[11]), i.e., losses that would occur using a nebulizer together with a spray chamber are avoided. Beside these advantages, this technique can also be used to analyze local and transient effects inside the ICP.[12,13]

Inductively coupled plasmas have already been studied by numerical simulation since the 1970s; see, e.g., ref 14. The simulations provide deeper insight into conditions inside the plasma, e.g., on the temperature or electron density distributions.[15]

Received: July 5, 2011
Accepted: July 29, 2011
Published: July 29, 2011

The simulations were often performed for applications other than chemical analysis, e.g., to improve conditions for nanoparticle production.[16] Simulations were typically performed in "closed" torches, i.e., the torch goes through the whole calculation region; see, e.g., ref 17. In the simulations of Yang et al.,[18] the flow went into ambient gas, but still, the radial extension was limited to the torch diameter and no flow of the ambient gas was explicitly treated. For such conditions, the boundary conditions are typically set by analytical solutions of the vector potential as can be found in the book of Montaser and Golightly.[19] The use of an extended geometry for the electro-magnetic fields[20] allows the use of simpler boundary conditions. The present model takes into account the flow of the ambient gas and thus has a wider geometry which allows the use of the extended electric field boundary conditions. Details on the model are presented in the paper by Lindner and Bogaerts.[21]

In the present paper, this model is applied to a pure argon ICP and compared with experiments. Very similar conditions were used for the experiments and the simulation to allow a good comparison. It provides at the same time a validation of the model by the experiments and a deeper insight into the local conditions by the simulation.

Indeed, in this paper, specifically the coil region of the plasma is studied. This region is not very well experimentally accessible, and thus, investigations of it are not very common. It is, however, of interest because the most important sample transformation processes (desolvation, atomization) are carried out here. Additionally, it is important for end-on ICP-OES, since here, the emission from the central channel of the plasma is detected if the injector gas flow rate is not too high. More specifically, the effect of injector gas flow rate on the plasma temperature inside the central channel using the line-to-background-ratio method[22] and the gas flow pattern inside the plasma are investigated. These parameters have strong influence on, e.g., the desolvation behavior of the droplets injected into the plasma and the resulting signal height and length. Additionally, the simulations are used to predict conditions for a good analyte transport through the plasma, by studying the effect of different injector diameters, injector gas flow rates, and injector gas compositions, i.e., helium/argon mixtures.

EXPERIMENTAL, SIMULATION, AND THEORETICAL BACKGROUND

Information on the experimental setup, the simulation model, and the theoretical background on the temperature determination from the line-to-background ratio are available in the Supporting Information for this article.

RESULTS AND DISCUSSION

Plasma Temperature. From the end-on measured and simulated line-to-background ratios, the effective temperatures [i.e., the average from the local emissivities of the inhomogeneous plasma and the light collection efficiency of the setup (see also the Supporting Information)] were calculated using eq S4 (see the Supporting Information). The result is displayed in Figure 1. The results of the simulation and the experiment show good agreement, i.e., less than 3% deviation, for injector gas flow rates of 0.5 L/min and less. For the torch under study here, i.e., with an injector diameter of 1 mm, the analytically relevant flow rate for the analysis of relatively large droplets (i.e., about 50 μm)[24]

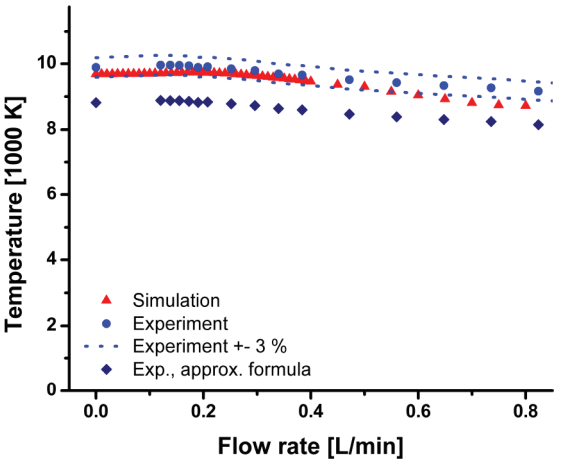

Figure 1. Simulated and experimental temperatures determined from the line-to-background ratios at different injector gas flow rates using eq S4 (see the Supporting Information) and the approximative formula given in ref 23.

ranges from about 0.2 to 0.3 L/min for pure argon. It is clear that simulation and experiment are in especially good agreement within this range. For the higher gas flow rates of up to 0.8 L/min, the agreement of simulation and experiment is slightly worse, but the deviations in temperature do never exceed 6%. We believe that the simulation results are still of reasonable accuracy here, but they have to be treated with more care. In the paper of Galley and Hieftje,[23] an approximative formula is provided to determine the temperature from the line-to-background ratio. That formula yields about 10% lower temperatures than the more extended equation used in the present study. Thus, the use of different equations results in larger deviations than obtained from the comparison of experiment and simulation. Consequently, a comparison of simulation and experimental results from literature needs to be considered with caution, especially if the equation, its assumptions, and all relevant parameters are not given explicitly. For instance, the value of ξ (see eqs 2 and 4 in the Supporting Information) for argon at a wavelength of 430 nm from the article of Schlüter[25] is about 1.8. In the paper of Hofsaess,[26] significantly lower values are given for the same parameter (see Table S3 in the Supporting Information). We used the latter reference for our calculations because, in that paper, a temperature dependence of ξ was given and a better wavelength-dependent resolution was provided. The use of the different parameters has an effect of a few percent on the resulting temperature values.

In eq S5 (see the Supporting Information), a fit function for the ionization potential reduction is given. Although this may not have a strong effect on the ionization of argon (it is below ~0.03 eV), it has an effect of a few percent on the resulting temperature from eq S4 (see the Supporting Information). Thus, this value may not be neglected for determining the temperature from the line-to-background ratio. Note, that in principle the given eq S5 (see the Supporting Information) is only valid for pure argon plasmas at atmospheric pressure in LTE.

In our opinion, there are two main origins for the deviations between the temperatures obtained by simulation and experiment. First, in the higher flow rate regime, the transition from laminar to turbulent gas flow regime comes close. Indeed, the Reynolds number *Re* of the gas flow in the injector tube for 0.8 L/min is about 1700 and the critical Reynolds number is 2300.

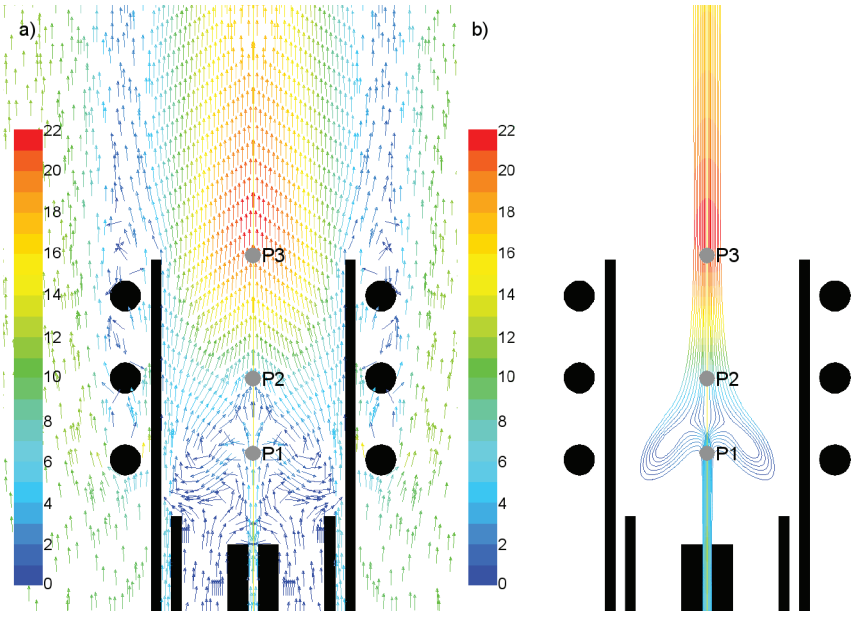

Figure 2. (a) Calculated vector plot of the velocity distribution (in m/s) for an injector gas flow rate of 0.22 L/min. (b) Corresponding calculated path lines originating from the injector inlet, colored by velocity in m/s. The detection heights P1, P2, and P3 from the experiments for the mean velocity determination (see Figure 4 below) are also displayed. "Path 1" is between P1 and P2; "path 2" is between P2 and P3.

The applied model does not cover turbulence, and it becomes less reliable when the critical Reynolds number is approached. The turbulence (or transitional flow) could result in stronger mixing of the relatively cold inner gas flow with the hot outer plasma. As a consequence, the center of the plasma becomes hotter in reality than found by the simulation.

Second, the simulation assumes axial symmetry. This assumption does not fully apply for the experimental plasma. Indeed, the load coil does not consist of ideal rings but has a spiral form. Simulations performed by Bernardi et al.[27] indicate that this affects the symmetry of the plasma. To take this effect into account, an extension of the model for three dimensions will be necessary.

Velocity Profiles. Figure 2a shows a vector plot of the calculated gas velocity. The plot also displays three experimental detection points at which side-on signals were taken. Note that the load coil of the plasma is a spiral in reality, and thus, the detection points located inside the coil rings were accessible. The flow close to the detection point P1 is not fully straight, but it leads outward. In contrast to that, the flow is rather straight for the other two detection points P2 and P3. In Figure 2b the calculated path lines of the injector gas stream are depicted. The outer path lines form an eddy shape, i.e., they first lead in outward direction before they turn back toward the center, forced by the cool-gas flow. The inner path lines follow a more or less straight way through the plasma.

Figure 3 illustrates the measured Ca(II) emission signals obtained for different injector gas flow rates. As can be seen, the signal tail is very long for 0.208 L/min, whereas it is short for 0.314 L/min and higher. This indicates that the analyte is not transported in a straight way through the plasma for low flow rates but is captured in the eddies formed in the upstream part of the plasma as shown in Figure 2. Furthermore, the signal intensity rises for flow rates higher than 0.208 L/min, indicating a more efficient sample introduction into the plasma. However, there is also a dramatic spatial shift of the onset of sample atomization

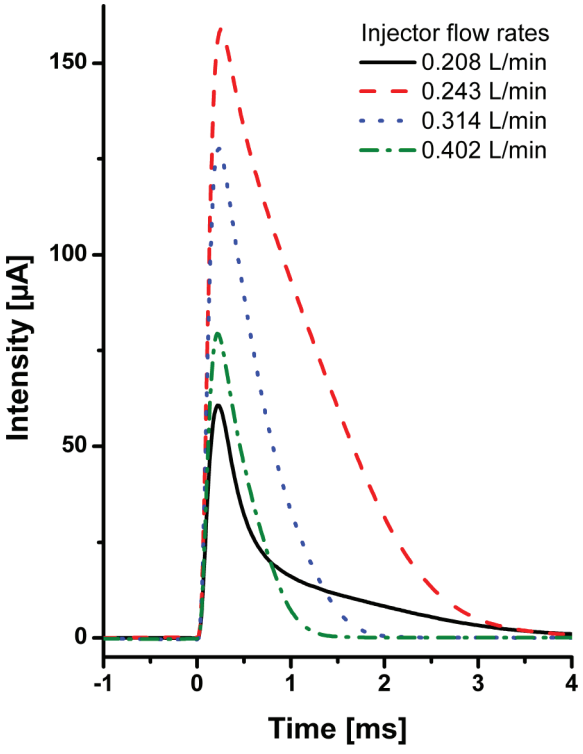

Figure 3. End-on measured Ca(II) emission signals at various injector gas flow rates.

downstream the ICP if the injector gas flow rate is increased; see Figure 5 and Murtazin et al.[24] This shift and the reduced light collection efficiency (see Figure S2 in the Supporting Information) are responsible for the decrease of the analyte signal for gas flow rates larger than ~0.243 L/min.

For the two paths, i.e., from the height of P1 to the height of P2 ("path 1") and from P2 to P3 ("path 2"), the mean velocity was

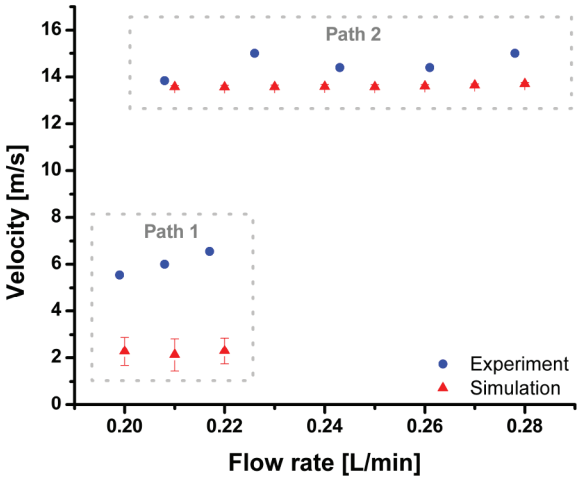

Figure 4. Mean velocity determined from simulation and experiment for two different regions in the plasma, i.e., "path 1" corresponds to the region between the detection heights P1 and P2, and "path 2" is between P2 and P3. See also Figure 2 for the position of these detection heights P1, P2, and P3.

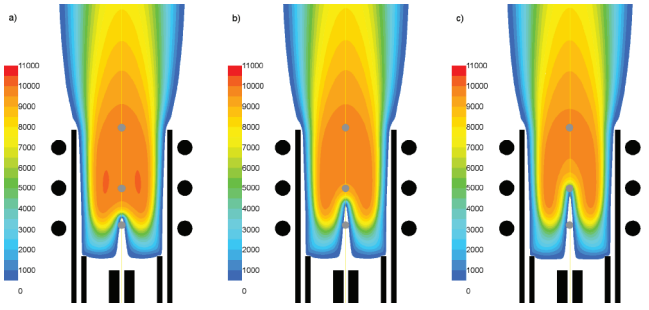

Figure 5. Simulated temperature distributions of the plasma for injector gas flow rates of (a) 0.22, (b) 0.30, and (c) 0.40 L/min. The color scale is in K. The gray points denote the same positions P1, P2, and P3, respectively, as in Figure 2.

determined for different flow rates (see also Table 1). The results are shown in Figure 4. The velocities for "path 1" are significantly lower than for "path 2" in both the simulation and the experiment. The range of investigated flow rates for "path 1" was limited by the range where proper signals could be taken at P1 in the experiment.

The velocities obtained from the path lines of the simulation show a large variation for "path 1", which is indicated by "error bars" in Figure 4. This variation originates (among others) from the different path lengths of the different path lines (cf., Figure 2). The length for the calculation of the mean velocity was—as in the experiment—the distance between P1 and P2; see Table 1. Since this path is significantly shorter than the path that is actually taken, the mean velocity calculated in this way is significantly reduced compared to the real velocity obtained in the simulation.

The simulations exhibit already a cool region (below 550 K) on the axis at P1 for the low flow rates studied for "path 1"; cf., Figure 5a. Thus, effectively no radiation would be emitted from there. However, in this range of the flow rate, path lines lead from a hot position between P1 and P2 backward (i.e., upstream; see Figure 2b) to the same axial but further outward position as P1. Thus, the experimental signals could also originate from outer

Table 1. Parameters of the Paths for the Velocity Determination[a]

	path 1	path 2
min position	−18.9 mm TT	−11.6 mm TT
max position	−11.6 mm TT	+0.4 mm TT
path length	7.3 mm	12 mm
flow rate range	0.20−0.22 L/min	0.21−0.28 L/min
mean velocity (exptl)	6.0 m/s	14.5 m/s
mean velocity PL (simul)	2.2 m/s	13.6 m/s

[a] TT, relative to torch top; PL, path lines.

plasma regions instead of the central part. The experiments cannot easily distinguish between the two possibilities—as stated in the Supporting Information, light is collected from the plasma along 13 mm in the radial direction through the plasma. Thus, the collected light may not originate from the center of the plasma but from the (backward flowing) borders of the central channel. In this case, the time delay is shorter between the measured signals at P1 and P2 in the experiment than expected from the simulation. First, the distance from the evaporation place (EP) to P2 (EP expected shortly behind the plasma "start" on the axis) is shorter than $\overline{P1P2}$. Second, a part of the analyte travels back from the EP to the height of P1 while the other travels further from EP to P2 during the same period of time. As a result the time delay between the side-on signals at P1 and P2 is shortened further, increasing the experimental mean velocity. This could explain why the calculated velocity for "path 1" is so much lower than the experimental value.

The velocity of "path 2" is significantly higher than that for "path 1" both in the simulated and measured results. Thus, the gas accelerates significantly downstream of P2. This can also be seen in Figure 2. Indeed, the gas is heated up by the power coupled into the plasma which results (due to conservation of energy, mass, and momentum) in the increased velocity. Different to "path 1", straight path lines are found, and the experimental and simulated results yield similar values in this region. Moreover, the velocity is effectively constant in the range of flow rates under study. Furthermore, the different path lines in this region exhibit the same velocities as can be seen from Figure 2 (note that the "error bars" in Figure 4 are smaller than the symbols), i.e., there is a homogeneous transport over a radial range of a few millimeters for "path 2". Consequently, the analyte follows well the general flow of the gas. As a consequence, the signal (e.g., from a single droplet) will not produce a long dispersion even if the analyte has diffused over a significant lateral cross section. Hence, different elements are detectable simultaneously even though lighter elements diffuse more easily than heavy ones. Nevertheless, note that signal prolongations and fractionation could still originate from upstream eddies.

Simulation of the Effect of Different Injector Diameters. As was shown in Figure 2, the path lines deviate at least partially from a straight way through the plasma when low injector gas flow rates are applied. In order to understand this effect better, simulations were run for different injector tube diameters while all other parameters were unchanged. The other conditions were also kept the same as described in Table S2 in the Supporting Information. The maximum injector gas flow rate used was dependent on the respective injector diameter. The conditions were analyzed in terms of when a proper transport of analyte through the plasma will occur.

The change of the injector tube diameter would experimentally require the change of at least the injector tube or even the

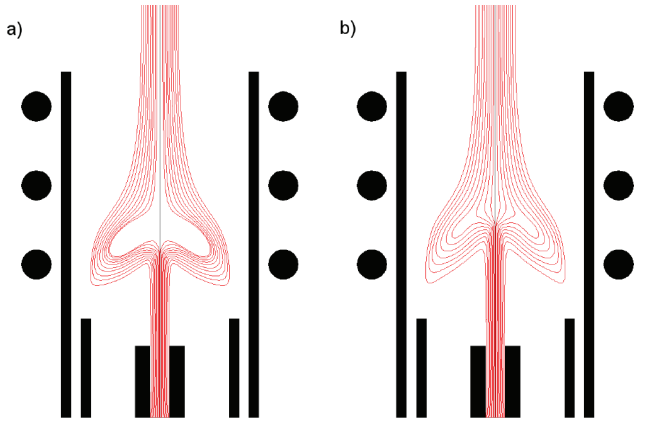

Figure 6. Path lines originating from the injector for an injector diameter of 2 mm and flow rates of (a) 0.40 and (b) 0.48 L/min.

whole torch. This means that new optimization and alignment would have been necessary each time the torch is changed. This work is time-consuming, and variations with respect to previous setups are very likely. Therefore, the effect of different injector diameters was not experimentally investigated but only theoretically. Indeed, numerical simulations allow a relatively easy analysis of the different setups.

In ICP spectrometry often injector gas flow rates in the order of 1 L/min are used, whereas for the present torch geometry significantly lower flow rates are the optimum.[24] Therefore, we looked for a criterion that gives a clear indication for such differences.

Figure 6 shows the path lines originating from the injector for two representative flow rates. One can distinguish two important regimes. For low flow rates (see Figure 6a), the path lines first flow straight into the coil region, but then they turn toward the outer positions of the torch. For higher flow rates, at least some part of the path lines penetrates through the plasma in a rather straight way. The amount of straight path lines increases with increasing flow rate. This behavior has important impact on the analysis. The analytes are usually situated in small droplets or particles that follow the path lines very well. As a result, the analyte will be transported toward the outer regions of the plasma in the case of low flow rates, where the droplets or particles will evaporate and diffuse in a large volume. Hence, they will not reach the detection point properly and thus will not be measured in a typical side-on configuration where the detection point is further downstream, outside the torch. For the higher flow rates, path lines lead in a straight way through the plasma and will take the analyte with them to the detection point where they are measured. For end-on measurements, the change of path line behavior has strong impact on the length of the signal, as was shown above. The signal tail is long for the low flow rates, whereas it is short for higher injector gas flow rates.

The transition from one flow behavior to the other occurs rather abruptly with increasing flow rate. In the following, we will call this flow rate the "transition flow rate" (TFR), and data for the TFR for different values of the injector diameter are presented in Table 2. It is obvious that the TFR increases with the injector diameters (see Figure 7) which means that, for larger injector diameters, a reasonable analysis is only possible at sufficiently large flow rates. This is an explanation why the flow rates typically applied in the literature are higher than the optimum values in the

Table 2. Calculated Transition Flow Rates (TFR) for Different Values of the Injector Diameter (d_{Inj}) and Injector Gas Compositions[a]

d_{Inj} [mm]	TFR [L/min]	η_{max} [μPa s]	ρ [kg/m^3]	gas	α
0.5	0.10	262	1.62	Ar	1.10
1.0	0.21	262	1.62	Ar	1.15
1.5	0.31	262	1.62	Ar	1.13
2.0	0.44	262	1.62	Ar	1.20
2.5	0.62	262	1.62	Ar	1.36
1.0	0.50	269	0.64	33% Ar 67% He	1.06
1.0	0.70	273	0.41	17% Ar 83% He	0.93

[a] Also given are the maximum viscosity (η_{max}) on the axis, the injector gas density (ρ) at 300 K, and the correction factor α for eq 2.

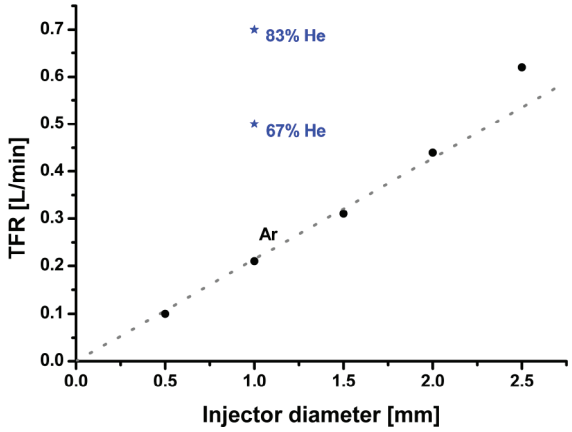

Figure 7. Calculated transition flow rates (TFR) as a function of the injector diameter. The circles denote the cases for pure argon, the stars denote helium−argon mixtures (in mole fractions) as injector gas.

torch geometry under study, because the present torch has a smaller injector diameter than typically reported in literature. One can also see from Figure 7 that the TFR is linearly proportional to the injector diameter for pure argon, although there is some deviation for an injector diameter of 2.5 mm. On the other hand, the required flow rate for helium−argon mixtures strongly deviates from that of pure argon as shown for an injector diameter of 1 mm in Figure 7. This indicates that the TFR is strongly dependent on the relative composition of the central gas (i.e., the resulting density and viscosity; see below and Table 2). This observation is important for practical applications because its means that in pure Ar, lower flow rates than for He/Ar mixtures are applicable for efficient analysis of small droplets as produced by nebulizers.

The injection of single large droplets has the advantage that the analyte is not distributed over the whole injector tube cross section but is situated only in the center of the tube. Hence, it is sufficient that only a part of the path lines goes straight through the plasma. Additionally, the droplets are rather heavy and they can deviate significantly from the path lines. In this way, they can more efficiently be injected into the plasma even if the path lines have a bent shape.

Origin of the Transition Flow Rate. In order to understand better the origin of the TFR, the path lines of the injector gas are plotted for the case of 0.20 L/min injector gas flow rate and an injector diameter of 1 mm in Figure 8, together with the contours of the viscosity. It is clear that the path lines follow the contours

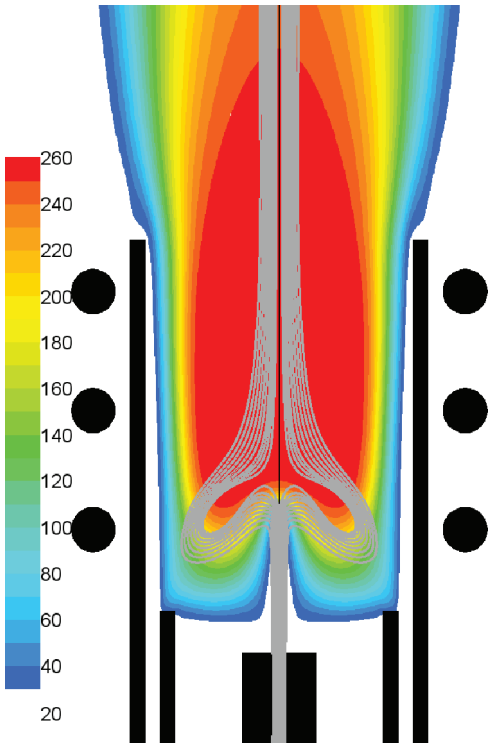

Figure 8. Path lines of the injector gas for a flow rate of 0.20 L/min displayed together with the viscosity. The viscosity is given in μPa s.

of the viscosity. Indeed, the central path lines reach just the maximum viscosity value for flow rates just below the TFR. This finding indicates that the viscosity is one major parameter for the TFR.

The existence of a TFR suggests the existence of a force balance, while the dependence on viscosity and the linear relation on the injector diameter (see above) suggest the Stokes drag force as one constituent. The TFR is, furthermore, related to the movement of the injector gas which could be regarded as an entity having a diameter d_{Inj}. The force that is evoked by the flowing injector gas is the dynamic force. Then, the force balance at the TFR becomes

$$\frac{1}{2}\rho v^2 A \approx \alpha 3\pi\eta_{max} v d_{Inj} \quad (1)$$

where α is a correction factor to take into account that the "injector gas entity" is not a solid sphere. The other symbols are injector gas density ρ, injector gas velocity v, cross section A, maximum plasma viscosity η_{max}, and the injector diameter d_{Inj}. Equation 1 can be rewritten in the following form:

$$\frac{1}{2}\rho \dot{V} \approx \alpha 3\pi\eta_{max} d_{Inj} \quad (2)$$

where $vA = \dot{V}$ is the volume flow rate through the injector.

In Figure 9, the correction factor α is displayed versus the injector diameter. As can be seen, it is close to one for the different injector diameters for pure argon but also for the different He/Ar mixtures investigated as injector gas. Thus, eq 2 can be used, even with $\alpha = 1$, to estimate the minimum required flow rate, i.e., the TFR, at which good transport through the plasma starts for different injector diameters and different injector gas mixtures.

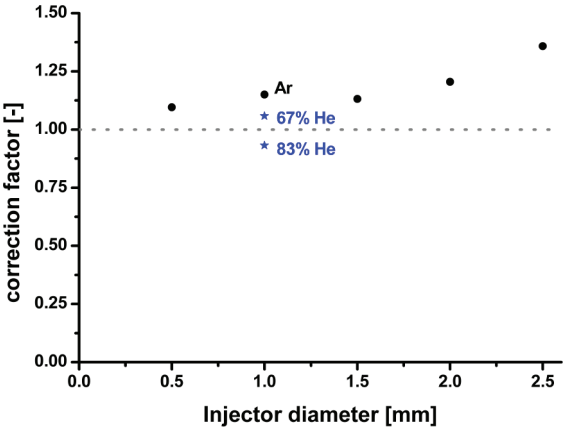

Figure 9. Correction factor α of eq 2 vs injector diameter. The circles denote pure argon, and the stars denote helium−argon mixtures (in mole fractions) as injector gas.

CONCLUSIONS

Calculation results of a model developed recently for an ICP[21] are presented and compared to experimental results obtained at very similar conditions to ensure comparability. The measured and simulated temperatures deviate less than 3% for injector gas flow rates smaller than 0.5 L/min and an injector diameter of 1 mm. As the analytically relevant flow rate ranges between 0.2 and 0.3 L/min for this injector diameter, this means that good agreement was found especially for the most important range of flow rates for the analysis of droplets of about 50 μm.[24]

Close to the region where the injector gas reaches the plasma, eddy structures are present in the flow. These affect the movement of the injector gas, but the influence is less pronounced for higher flow rates. The mean velocity in axial direction for the analyte is rather low in this region. Inside the plasma a straight transport is present, and similar velocities are found across a few millimeters of radial positions. Thus, good analyte transport occurs and little signal dispersion is induced here. The mean velocities can effectively be determined from the path lines in this region.

The behavior of the flow lines was analyzed for different injector diameters. The path lines show a clear transition in behavior as a function of increasing injector gas flow rate. For flow rates below that transition point, the path lines show a strong deviation from a straight way, i.e., leading toward the outer regions of the torch, which induces small and long analyte signals if single droplets are injected. For higher flow rates, some of the path lines lead in a straight way through the plasma and the number of straight path lines increases with increasing flow rate. In this way, small particles or droplets are led directly into the plasma where they are evaporated and excited. Furthermore, the analyte is driven toward the detection point where it can be measured in typical side-on configurations. For the flow rates below the transition point, the small particles and droplets are transported to the periphery of the plasma where they evaporate at outer regions. They diffuse into a large volume and will not be detected in side-on configurations. Additionally, analyte will be trapped inside eddies that are situated in the upstream part of the plasma. In the end-on configuration, analyte will thus be present in the detection volume for a rather long time producing a strong signal dispersion.

It should be noted that the transition flow rate will not be the optimum flow rate for analysis. The optimum flow rate will be

somewhat higher. The transition flow rate increases with larger injector diameters, and thus, also the optimum flow rate will be higher for a large injector than for smaller ones. Note that also other boundary conditions can influence the optimum flow rate. Some nebulizers require a sufficiently high flow rate to produce a proper aerosol. As a consequence, it can be necessary to choose the right injector diameter to achieve optimum conditions for both the nebulizer and the inductively coupled plasma. Single-droplet generators as used in the present experiments do not depend on the gas flow rate for droplet production. The gas velocity is nevertheless a relevant parameter for the droplet transport which can be adapted for the transport/injector tube diameter used. Smaller diameters require a lower minimum flow rate.

Finally, a simple relation (eq 2) was found to estimate this transition flow rate for a given injector diameter. It allows us, for instance, to estimate for which helium−argon ratio and which flow rate value in the injector gas a good transport through the plasma can be expected. This value is dependent on the injector diameter and the density of the injector gas used.

■ ASSOCIATED CONTENT

Supporting Information. Additional information as noted in text. This material is available free of charge via the Internet at http://pubs.acs.org.

■ AUTHOR INFORMATION

Corresponding Author
*E-mail: annemie.bogaerts@ua.ac.be.

■ ACKNOWLEDGMENT

The authors thank Maryam Aghaei for setting up some of the calculations. This work was financially supported by the IAP-P6/42 project "Quantum Effects in Clusters and Nanowires" and by the Deutsche Forschungsgemeinschaft. The calculation support of the core facility CALCUA, provided by the University of Antwerp, is gratefully acknowledged.

■ REFERENCES

(1) Olesik, J. W. *Anal. Chem.* **1991**, *63* (1), 12A–21A.
(2) Bings, N. H.; Bogaerts, A.; Broekaert, J. A. C. *Anal. Chem.* **2010**, *82*, 4653–4681.
(3) Engelhard, C. *Anal. Bioanal. Chem.* **2011**, *399*, 213–219.
(4) Koch, J.; Berndt, H.; Schaldach, G.; Niemax, K. *Anal. Chem.* **2004**, *76* (7), 130A–136A.
(5) Todolí, J.-L.; Mermet, J.-M. *J. Anal. At. Spectrom.* **2001**, *16*, 514–520.
(6) Garcia, C. C.; Lindner, H.; Niemax, K. *J. Anal. At. Spectrom.* **2009**, *24*, 14–26.
(7) Orlandini v. Niessen, J. O.; Schaper, J. N.; Petersen, J. H.; Bings, N. H. *J. Anal. At. Spectrom.* **2011**, *26*, 1781−1789.
(8) Garcia, C. C.; Murtazin, A.; Groh, S.; Horvatic, V.; Niemax, K. *J. Anal. At. Spectrom.* **2010**, *25*, 645–653.
(9) Garcia, C. C.; Murtazin, A.; Groh, S.; Becker, M.; Niemax, K. *Spectrochim. Acta, Part B* **2010**, *65*, 80–85.
(10) Kaburaki, Y.; Shigeta, K.; Iwai, T.; Miyahara, H.; Okino, A. Development of droplet direct injection ICP-QMS/TOFMS for single cell analysis. Presented at the European Winterconference on Plasma Spectrochemistry, Zaragoza, Spain, 2011.
(11) Groh, S.; Divakar, P. K.; Garcia, C. C.; Murtazin, A.; Hahn, D.; Niemax, K. *Anal. Chem.* **2010**, *82*, 2568–2573.
(12) Groh, S.; Garcia, C. C.; Murtazin, A.; Horvatic, V.; Niemax, K. *Spectrochim. Acta, Part B* **2009**, *64*, 247–254.
(13) Olesik, J. W. *Appl. Spectrosc.* **1997**, *51* (5), 158A–175A.
(14) Eckert, H. U. *J. Appl. Phys.* **1977**, *48* (4), 1467–1472.
(15) Shigeta, M.; Sato, T.; Nishiyama, H. *Thin Solid Films* **2003**, *435*, 5–12.
(16) Schubert, H. PhD Dissertation. Spektroskopische Untersuchung und Modellierung einer zur Erzeugung von ZrO2-Nanopartikeln verwendeten HF-Entladung. Dissertation, Heinrich-Heine-Universität, Düsseldorf, Germany, 2003.
(17) Holclajtner-Antunović, I.; Raspopović, Z.; Georgijević, V.; Tripković, M. *Plasma Chem. Plasma Proc.* **1997**, *17* (3), 331–352.
(18) Yang, P.; Horner, J. A.; Sesi, N. N.; Hieftje, G. M. *Spectrochim. Acta, Part B* **2000**, *55*, 1833–1845.
(19) Montaser, A.; Golightly, D. W. *Inductively Coupled Plasmas in Analytical Atomic Spectrometry*, 2nd ed.; VCH Publishers: New York, 1992.
(20) Xue, S.; Proulx, P.; Boulos, M. I. *J. Phys. D: Appl. Phys.* **2001**, *34*, 1897–1906.
(21) Lindner, H.; Bogaerts, A. *Spectrochim. Acta, Part B* **2011**, *66*, 421–431.
(22) Bastiaans, G. J.; Mangold, R. A. *Spectrochim. Acta, Part B* **1985**, *40* (7), 885–892.
(23) Gallay, P. J.; Hieftje, G. M. *Spectrochim. Acta, Part B* **1993**, *48* (14), E1725–E1742.
(24) Murtazin, A.; Groh, S.; Niemax, K., to be submitted for publication.
(25) Schlüter, D. *Z. Astrophys.* **1965**, *61*, 67–76.
(26) Hofsaess, D. *J. Quant. Spectrosc. Radiat. Transfer* **1978**, *19*, 339–352.
(27) Bernardi, D.; Colombo, V.; Ghedini, E.; Mentrelli, A. *Eur. Phys. J. D* **2003**, *22*, 119–125.